

Therapeutic Magnetic Microcarriers Guided by Magnetic Resonance Navigation for Enhanced Liver Chemoembolization: A Design Review

PIERRE POUPONNEAU, GAËL BRINGOUT, and SYLVAIN MARTEL

NanoRobotics Laboratory, Department of Computer and Software Engineering and Institute of Biomedical Engineering, Ecole Polytechnique de Montréal (EPM), C.P. 6079, Succ. Centre-ville, Montreal, QC H3C 3A7, Canada

(Received 11 September 2013; accepted 9 January 2014; published online 17 January 2014)

Associate Editor Agata A. Exner oversaw the review of this article.

Abstract—This review paper describes the past, present and future design of therapeutic magnetic carriers (TMMC) being guided in the vascular network using a novel technique known as magnetic resonance navigation (MRN). This targeting method is an extension of magnetic resonance imaging (MRI) technologies. MRN, based on magnetic gradient variation, aims to navigate carriers in real-time along a pre-planned trajectory from their injection site to a targeted area. As such, this approach should minimize systemic distribution of toxic agents loaded into the carriers and improve therapeutic efficacy by delivering a larger proportion of the drug injected. MRN-compatible carriers (shape, material, size, magnetic properties, biocompatibility) have to be designed by taking into consideration the constraints of the medical task and MRN. In the past, as a proof of concept of MRN feasibility, a 1.5-mm ferromagnetic bead was guided in the artery of a living swine with a clinical MRI system. Present day, to aim at medical applications, TMMC have been designed for targeted liver chemoembolization by MRN. TMMC are 50- μm biodegradable microparticles loaded with iron-cobalt nanoparticles and doxorubicin as an antitumor drug. TMMC were selectively guided to the right or left liver lobes in a rabbit model with a clinical MRI scanner upgraded with steering coils. To treat human liver tumor, according to the theoretical MRN model, future TMMC design should take into consideration magnetic nanoparticle properties (nature and loading), MRN platform performances (gradient amplitude and rise time) and vascular hepatic network properties (blood flow velocity and geometry) to optimize the carrier diameter for efficient chemoembolization.

Keywords—Magnetic tumor targeting, Magnetic resonance imaging (MRI), Magnetic nanoparticles, Microparticles, Drug delivery.

Address correspondence to Sylvain Martel, NanoRobotics Laboratory, Department of Computer and Software Engineering and Institute of Biomedical Engineering, Ecole Polytechnique de Montréal (EPM), C.P. 6079, Succ. Centre-ville, Montreal, QC H3C 3A7, Canada. Electronic mail: sylvain.martel@polymtl.ca

INTRODUCTION

Autonomous medical micro/nanodevices are currently developed to be guided from their injection site in the vascular network to targeted areas according to a pre-planned trajectory.^{1,15,27,35} These systems should improve the targeting of the medical task and minimize side effects such as systemic distribution of toxic agents or blood vessel damages. To navigate in the blood flow according to a trajectory, these devices require a propulsion system. Furthermore, they should be tracked in real-time to adjust their position in the vascular network. One major challenge in this field is the reduction of the propulsion system and its power supply to reduce the size of the device for medical interventions in narrower blood vessels.^{1,27} To avoid embedded batteries, which limited the size of the device to the millimeter scale, it was proposed to use external power supply.^{27,33} Among many types of actuation methods investigated to control the microdevice navigation, the ones based on magnetism appear to be the best promising methods.^{15,27,39,41} The propulsion and the trajectory of the device are controlled by homogeneous and non-homogeneous magnetic fields. The applications investigated with this strategy are mainly for therapeutic treatments such as surgery,⁴⁹ drug,³⁸ or cell⁴⁵ delivery and for diagnostic such as capsule endoscopy²⁰ or contrast agent.¹¹ Different micro/nano carrier designs are currently investigated *in vitro*: microrobots, microparticles, magnetic cells or nanoparticles.^{1,11,15,20,35,45}

The size of these magnetic devices depends on several parameters: the dimensions of the targeted vascular network, the blood flow velocity, the properties of the magnetic field applied (field and gradient amplitude) and the device characteristics (shape, volume and magnetic behavior).^{27,30,40} Furthermore, the

displacement of a magnetic material according to fixed gradient amplitude will be more effective if the saturation magnetization (M_s) is reached. However, when a single external magnet to the body is used, the magnetic field in the tissues decreases sharply with the distance between the magnet and the device.^{9,10,37} Hence, this approach remains limited to superficial organs mainly.^{10,31} Furthermore, due to these design constraints mentioned above and the blood flow velocity, the application of this approach to target deep tissues remains highly challenging and is not used in clinical practice.^{3,13,24,36}

To overcome these limitations, a new approach, referred to as magnetic resonance navigation (MRN), has been proposed to steer and track along a pre-planned trajectory in real-time untethered micro-devices or microcarriers using a magnetic resonance imaging (MRI) scanner.²⁷ The permanent homogenous magnetic field (1.5 T or higher) of the clinical scanner enables to reach the saturation magnetization of ferromagnetic materials throughout the whole patient.^{27,40} Hence, the problem of weaker magnetic field in deep tissues observed with a single external magnet can be overcome. For navigation in the vascular network, the three orthogonal gradient coils inside the bore of an MRI system, typically used for slice selection and signal encoding during MR imaging, can also generate a three dimensional directional magnetic force (\mathbf{F}) sufficient to propel an object made of ferromagnetic material. This force is proportional to the amplitude of the gradient vector according to Eq. (1):

$$\mathbf{F} = R(V\mathbf{M} \cdot \nabla)\mathbf{B}_z, \quad (1)$$

where R is the duty cycle of gradient generation, V the volume of the ferromagnetic object, \mathbf{M} the magnetization of the material, \mathbf{B}_z the magnetic field in the z direction, and ∇ the vector differential operator.²⁷ This propulsion force depends on the carrier and MRN platform properties. To navigate the carrier according to a pre-planned trajectory, the propulsion force must overcome a drag force induced by the blood flow. Moreover, the imaging capability of the system allows the tracking of device in real-time.¹⁴ The tracking step should be interleaved with the steering step to adjust the force according to the carrier position to follow the pre-planned trajectory.

This strategy is mainly investigated to improve drug delivery. For this purpose, the drug is combined with MRN-compatible carrier. To be successfully steered to the region of interest, the carrier has to be designed (shape, material, size, M_s , biocompatibility) by taking into consideration several constraints such as the MRN platform properties, the therapeutic task and the vascular network parameters.

This paper reviews the design of MRN-compatible carriers from the first *in vivo* MRN in a swine artery as a proof-of-concept (past) to the first medical application for hepatocellular carcinoma (HCC) chemoembolization (present) where therapeutic magnetic microcarriers (TMMC) were steered in the rabbit hepatic artery to target the right or left liver lobes. The last section of the paper introduces the future TMMC design constraints for human scale intervention based on the MRN model.

Past Design

A 1.5-T clinical MRI scanner was used to validate *in vivo* the concept of MRN. A 1.5-mm magnetic chrome steel bead was driven in real-time in the carotid artery of a swine according to several way-points determined by the radiologist (Fig. 1).²⁷ A spherical shape was preferred over a spheroid shape as the drag forces are minimized since a ferromagnetic body tends to maintain its original orientation along the main field (often named B_0 field) inside the MRI bore. Peak velocities of the bead were in the range of 8–11 cm s⁻¹ when the blood flow was reduced with a balloon catheter. The magnetic properties of the bead, required for the steering, induced artifacts on MR images that overrun the size of the bead.¹⁴ Consequently, the exact localization of the bead in the blood vessel by MRI was unknown and thus the adjustment of the steering gradient amplitude required to control the carrier trajectory was not achieved. Hence, a controller and specific MRI and tracking sequences were designed to interleave steering and tracking sequences.^{8,14,28,47} The tracking sequences were adjusted to bypass MR susceptibility artifacts caused by the ferromagnetic material (Fig. 1).

The clinical scanner used during the experiments generated maximum gradient amplitude of 40 mT m⁻¹. This amplitude limited the propulsion force and thus the carrier design to the millimeter scale.^{27,40} Furthermore, the bead was made of chrome steel to limit its corrosion in the blood vessels. However, this alloy did not exhibit the best M_s value. To reduce the size of the bead, a design study was conducted with several magnetic materials such as iron-cobalt (FeCo) alloys, neodymium-iron-boron (Nd-Fe-B) alloys, iron-nickel (FeNi) alloys and chrome steel alloys (SS 304L, 0.023% C, 18.22% Cr, 0.34% Si, 8.58% Ni, 1.79% Mn, 0.43% Mo).^{40,41} Instead of using SS 304L ($M_s \approx 186$ emu g⁻¹), the use of FeCo alloys such as Permendur (49% Fe, 49% Co, 2% V, $M_s \approx 230$ emu g⁻¹) could allow us to reduce the diameter of the bead by 26%. However, a biocompatibility study has shown that FeCo alloys

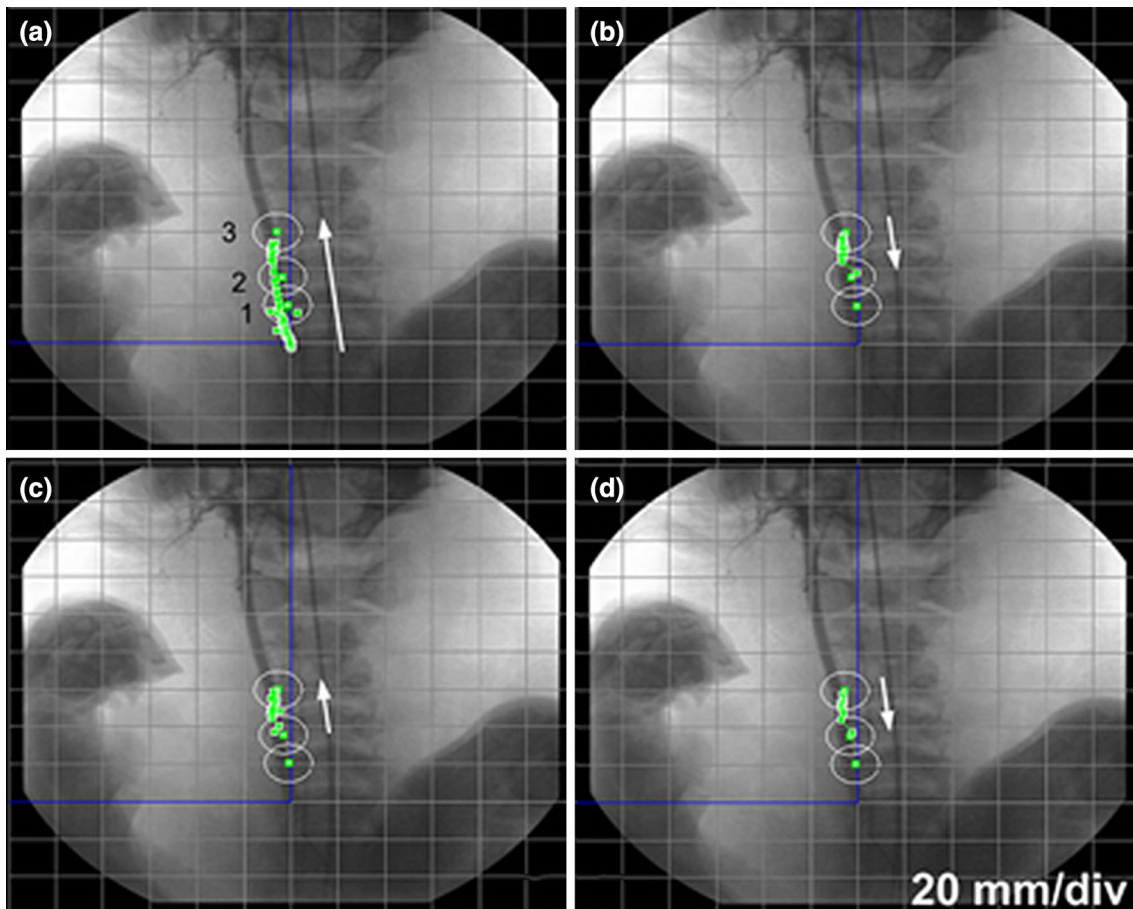


FIGURE 1. *In vivo* automatic navigation of a 1.5-mm ferromagnetic bead inside the carotid artery of a living swine. The trajectories are superimposed over an X-ray angiography. The line of dots over the artery shows real-time displacement of the bead. The circles (20 mm diameter) around each waypoint show precision tolerance region determined by the MRI tracking sequence. Arrows show the direction of displacement. On image (a), the bead travels through waypoints 1 and 2 and reaches the precision region of waypoint 3. Target waypoint changes from waypoint 3 to waypoint 2 (b). Images (c, d) show two subsequent round-trips as target waypoint switches from waypoint 2 to waypoint 3 alternatively (Reprinted with permission from Martel *et al.*,²⁷ (Copyright 2007, AIP Publishing LLC).

induced cytotoxic effects and they exhibited poor corrosion resistance resulting in a stoichiometric dissolution of the alloy in physiological media.⁴⁰ Hence, FeCo alloys should be used with a coating to prevent direct contact with physiological solutions.^{34,40,41}

Despite the use of materials exhibiting the best M_s value, the size of the carrier remained limited to the millimeter scale due to the limited gradient amplitude generated by the clinical scanner and the high velocity of the blood flow. Consequently, the medical applications were restricted to the main arteries, one of those application being the improvement of catheter guiding.¹⁶ To steer micrometer-scale carriers suitable for clinical applications, additional magnetic gradient amplitudes were required to compensate for the size reduction.²⁹ As such, the MRN platform was improved by adding gradient coils installed inside a clinical MRI scanner.^{26,29} With this upgraded MRN

platform, a gradient up to 400 mT m^{-1} was applied to steer $15\text{-}\mu\text{m}$ iron oxide (Fe_3O_4) microparticles.

Present Design

As a first clinical application, TMMC are MRN-compatible microcarriers designed for HCC nodules treatment by trans-arterial chemoembolization (TACE) (Fig. 2).³⁸ This liver tumor is characterized by the derivation of the blood supply from the hepatic artery.¹² HCC patients exhibit a poor prognostic outlook; near 70% can receive only palliative treatments.⁶ TACE, the most efficient palliative treatment, combines the injection by a catheter in the hepatic artery branches of an antitumor drug followed by the occlusion with microparticles of the blood vessels feeding the tumor. Recently, drug-eluting beads (DEB), which are microparticles sustaining drug release, were used to

reduce the systemic drug concentration. However, TACE efficacy remains limited by the lack of tumor targeting; the positioning of the catheter close to the tumor remains difficult and the distribution of the chemo-embolic agents is not controlled. This could induce damages to healthy cells and blood vessels. Hence, TMMC were designed by taking into consideration the hepatic vascular network properties and MRN and therapeutic constraints.^{38,39} As a proof-of-concept, these carriers had to be steered from their release in the hepatic artery to the right or left lobes of rabbit liver (Fig. 2). The therapeutic constraints of these carriers were the sustained release of the drug and the proper size for the embolization of tumor blood vessels.³⁸ Thus, these carriers took the form of biodegradable microparticles loaded with magnetic nanoparticles (MNP) and an antitumor drug (Fig. 2a).^{38,39}

A basic MRN model, based on the magnetophoretic (V_{mag}) and blood (V_{blood}) velocities, was used to design TMMC.^{29,38,40} V_{mag} corresponded to the transversal velocity acquired by the carrier under the magnetic gradient in a 1.5-T MRI scanner. V_{mag} (m s^{-1}) was calculated according to Eq. (2):

$$V_{\text{mag}} = \frac{f \times M_{\text{Snanoparticles}} \times V_{\text{TMMC}} \times \nabla B}{6\pi \times a \times \mu}, \quad (2)$$

where f was the concentration of encapsulated nanoparticles (% w/w), $M_{\text{Snanoparticles}}$ was the MNP saturation magnetization (A m^{-1}), V_{TMMC} is TMMC volume (m^3), ∇B is the applied magnetic steering gradient (T m^{-1}), a is the TMMC radius (m) and μ is the blood viscosity (0.0035 Pa s).³⁸ M_s was considered since

MNP reach saturation when located inside the tunnel of the MRI scanner (permanent magnetic field of clinical MRI system $\geq 1.5 \text{ T}$).^{27,40} V_{blood} was the longitudinal velocity acquired by the microcarrier drifted by the blood flow. To target a bifurcation, the longest path was considered. Hence, TMMC had to cross the artery radius. This assumption was chosen because this basic model did not take into consideration the blood flow velocity profile. Accordingly, from V_{mag} , the time required by TMMC to cross the artery radius, referred to as the steering time, was determined. From V_{blood} , the time required by the TMMC drifted by the flow to reach the bifurcation (t_{max}) was calculated. For MRN, the steering time should be lower than t_{max} .

The design study indicated that the TMMC mean diameter (\varnothing) should be $50 \mu\text{m}$ (Fig. 2b) to get a distal embolization without extravasation in the liver parenchyma and that the microparticles should contain 30% FeCo nanoparticles (w/w) to give adequate M_s for steering.³⁸ FeCo MNP were preferred to Fe_3O_4 nanoparticles because their M_s allowed reducing the magnetic content from 50 to 30% (w/w).³⁸ In practice, FeCo MNP ($\varnothing = 206 \pm 62 \text{ nm}$, $M_s = 202 \pm 6 \text{ emu g}^{-1}$) were coated with a graphite shell to keep their magnetic properties and to limit their oxidation.^{38,39,42} TMMC ($\varnothing = 53 \pm 19 \mu\text{m}$, $M_s = 72 \pm 3 \text{ emu g}^{-1}$) were loaded (w/w) with FeCo nanoparticles ($37 \pm 2.7\%$) and doxorubicin (DOX) ($3.2 \pm 0.5\%$) (Fig. 2b).³⁹ DOX is routinely used for the liver tumor treatment by chemoembolization.⁴⁴ To control the drug release, TMMC were biodegradable microparticles made of poly(D,L-lactic-co-glycolic acid) (PLGA).²³ These carriers exhibited a sustained release

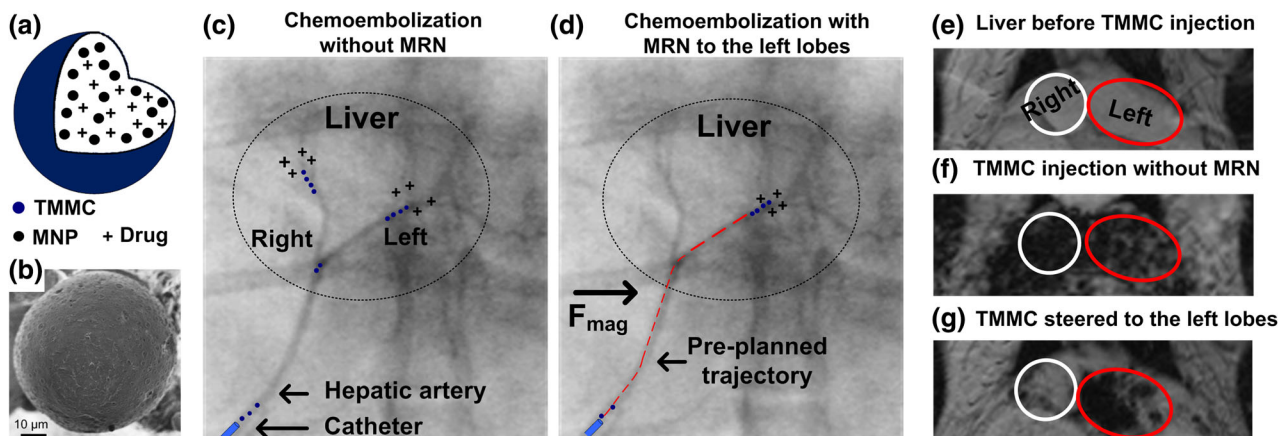


FIGURE 2. Targeted rabbit liver chemoembolization with TMMC. Image (a) corresponds to a schematic representation of TMMC loaded with MNP and an antitumor drug. Image (b) is a scanning electron microscopy image of TMMC. Images (c, d) are fluorescence images of the rabbit hepatic artery with superposed images of the TMMC distribution without (c) and with (d) MRN. On image (c), the microcarriers are released from the catheter in the artery and deliver to both lobes. Image (d) displays the targeting of the left bifurcation by MRN according to a pre-planned trajectory. Images (e–g) correspond to *in vivo* liver T2*-weighted gradient-echo MR images before (e) and after TMMC injection without (f) and with MRN (g). Without MRN, the right and left lobes are darkening, indicating the presence of TMMC in the whole liver. With steering to the left lobes, the right lobe appears mainly free of TMMC (Adapted from Pouponneau *et al.*,³⁹ NanoRobotics Laboratory, Ecole Polytechnique de Montréal).

of doxorubicin characterized by a burst release of 25% occurring within the first 5 min and after 3 days of elution, about 50% of the initial encapsulated DOX amount remains in TMMC.³⁹

Therapeutic magnetic carriers were steered *in vivo* in the rabbit hepatic artery (Figs. 2c and 2d).^{38,39} Under fluoroscopic visualization, 0.027-lumen catheter was placed in the proper hepatic artery (PHA) as far as possible from the right/left bifurcation. A balloon catheter (5 mm × 2 cm), placed in the abdominal aorta at the level of the celiac trunk, was inflated to reduce the blood flow velocity during TMMC injection. TMMC (40 mg) in saline solution (18 mL) were slowly injected (1.6 mL min⁻¹).^{39,43} For MRN, the animal model was placed between two steering coils perpendicular to the MRI tunnel (Fig. 3). Hence, the steering gradient amplitude, which depends on the distance between the coils, was limited by the size of the animal and varied from 271 to 303 mT m⁻¹ (Fig. 3b). These coils (100 kg each) were removed after

MRN to image the liver (Fig. 3c). The steering distance (Fig. 4a) corresponded to the distance between the catheter tip and the right/left hepatic artery bifurcation (Figs. 2c and 2d). The catheter position in the hepatic artery depended on the vascular anatomy and was adjusted to avoid spasms or artery thrombosis.¹⁹ The hepatic artery diameter varied from 1.1 to 1.3 mm (Fig. 4b).

The carrier and DOX distribution was significantly affected by the MRN compared to control (Figs. 2e–2g). The steering decreased significantly the carrier amount in the untargeted lobe. The steering efficiency (Fig. 4) was defined as the reduction of the carrier (or drug) dose in the untargeted area vs. the negative control (no MRN). This efficiency illustrates the potential of MRN to spare the healthy liver lobes during chemoembolization. The efficiency, evaluated by MR images (Figs. 2e–2g) and determined by histology analysis and assay of Co and DOX levels, varied from 12 to 49% (Fig. 4). When the steering

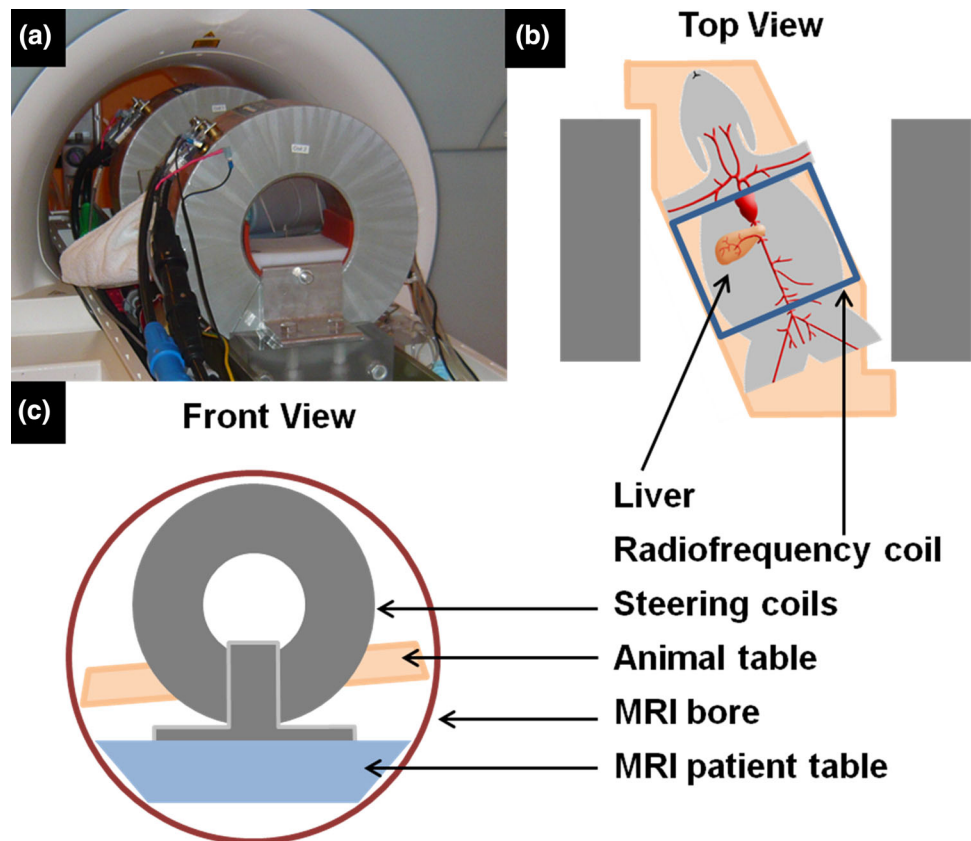


FIGURE 3. *In vivo* MRN platform used to steer TMMC in the rabbit hepatic artery to the right or left liver lobes. Image (a) corresponds to the MRN platform outside of the MRI tunnel. Images (b, c) represent schematic top and front views of the MRN platform, respectively. The animal model was placed on a table exhibiting several degrees of freedom. The animal position is adjusted to place the hepatic artery in the middle of the steering coils (x , y , z directions) to maximize the gradient amplitude. A radiofrequency (RF) coil is put on the animal to image the liver. The steering coils ($\varnothing = 55$ cm) are equipped with a current reversal switch and a power supply cooled down with a water cooler system. Depending on the rabbit size, the distance between these coils varies from 37 to 39 cm. Hence, the steering gradient amplitude varies from 271 to 303 mT m⁻¹ (NanoRobotics Laboratory, Ecole Polytechnique de Montréal).

distance increased, t_{\max} increased. Hence, TMMC had more time to cross the hepatic artery radius. In this case, the steering efficiency reached 49% (Fig. 4a). When TMMC were released close to the hepatic artery bifurcation, t_{\max} reduced. Hence, the steering efficiency was affected by the artery radius and then by the steering gradient (Figs. 4b and 4c).

Table 1 reports the theoretical diameter and theoretical volume of TMMC steered (%) according to the blood flow velocity in the rabbit hepatic artery for different *in vivo* steering efficiency. In the blank animal group (without TMMC injection), the mean velocity of the blood flow in the rabbit hepatic artery was measured by external Doppler ultrasound (US). This measure was not done in the groups with TMMC injection because it could induce spasm on the hepatic artery, probably related to the compression of the artery on the catheter by the US probe. The mean velocity measured varied from 24 to 48 cm s⁻¹ ($n = 3$). When the balloon catheter was inflated, the blood flow velocity was reduced from 50 to 70%. When the theoretical diameter of TMMC, which could be steered, decreased, the *in vivo* steering efficiency increased; the proportion of carrier steered increased. When the steering distance was above 60 mm, the blood flow velocity had a minor impact on the proportion of particles steered. However, when the catheter was placed close to the bifurcation, i.e., 20 mm, the blood flow velocity had a significant impact on the proportion of TMMC steered.

This *in vivo* study confirmed the appropriate design of TMMC based on the MRN model.³⁹ This model remains relatively basic but it can be used to evaluate if the MRN can be realized according to the properties of the vascular network and MRN platform. Furthermore, this model can be used to investigate the effects of several parameters on the TMMC design. To predict the *in vivo* steering efficiency, the model should integrate several parameters such as particle aggregation, arterial pulse on the blood flow and the hepatic artery geometry.^{4,29,38,39} Furthermore, the *in vivo* steering efficiency reported was impaired by the fact that the liver lobe embolization was not monitored in real-time; the steering coils were not compatible with the imaging sequences. Consequently, TMMC could have refluxed to the untargeted lobe because the targeted lobe was full of particles.

The MR imaging of TMMC was investigated.⁴³ TMMC induced a hypointense signal that overran the physical size of the sample on MR images. This signal, due to the nanoparticles embedded into the micro-particles, increased significantly with echo-time (TE) and sample amount. *In vivo*, without steering, contrast-to-noise ratio (CNR) values for the right and left lobes were similar. With MRN, the CNR in the targeted lobe was different from that in the untargeted lobe. TMMC accumulation in the liver (without MRN) was tracked in real-time with an 8-s T2*-weighted gradient-echo (GRE) sequence. Hence, to monitor the efficiency of future MRN, T2*-weighted GRE sequences with short

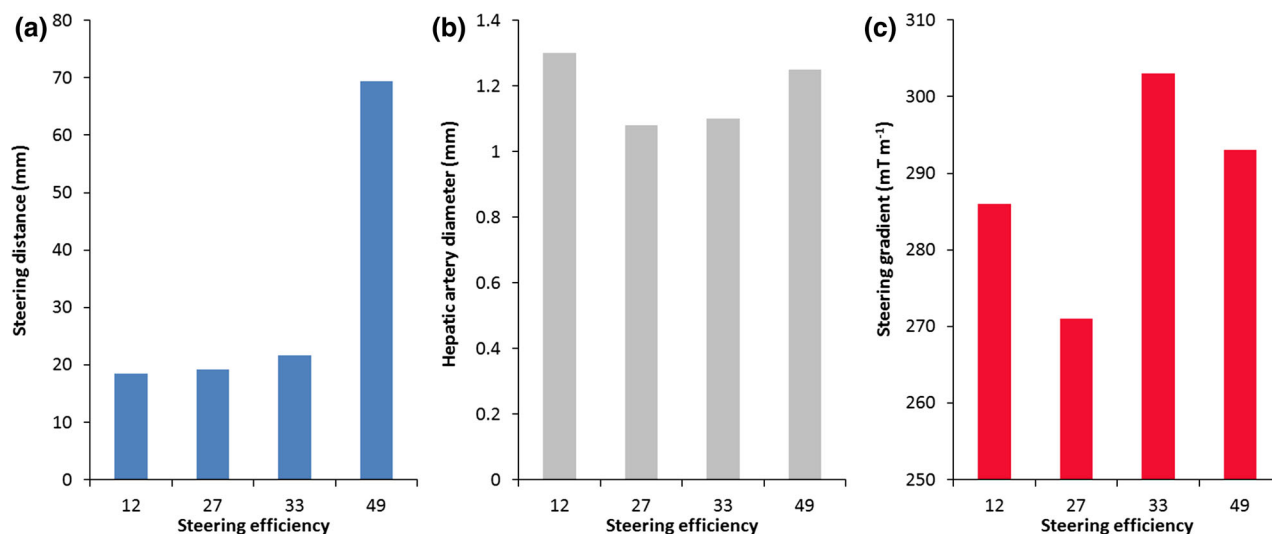


FIGURE 4. *In vivo* steering efficiency according to the steering distance (a), the hepatic artery diameter (b) and the steering gradient amplitude (c) ($n = 4$). Steering efficiency is defined as the reduction of the TMMC (or drug) dose in the untargeted area in the presence of magnetic steering vs. the negative control (no steering). An efficiency of 50% means that only 25% of the injected dose reach the untargeted lobe. When the steering distance is below 20 mm and the artery diameter is above 1.1 mm, the efficiency remains below 15%; TMMC have not the time to cross the artery radius before reaching the bifurcation. The steering efficiency increases from 27 to 33% by increasing the magnetic gradient amplitude up to 303 mT m⁻¹. The efficiency reaches 49% when the steering distance increases up to 69 mm. In such configuration, most of TMMC should have crossed the artery radius before reaching the bifurcation (NanoRobotics Laboratory, Ecole Polytechnique de Montréal).

TABLE 1. Theoretical diameter and theoretical volume (%) of TMMC steered according to the blood flow velocity in the rabbit hepatic artery for different *in vivo* steering efficiency.

<i>In vivo</i> steering efficiency (%)	Blood flow velocity (cm s ⁻¹)			
	7.5	15	22.5	30
12	32 μm (90%)	46 μm (63%)	56 μm (45%)	65 μm (39%)
27	30 μm (95%)	42 μm (73%)	51 μm (54%)	59 μm (45%)
33	27 μm (96%)	38 μm (83%)	48 μm (63%)	53 μm (54%)
49	16 μm (99%)	23 μm (97%)	28 μm (95%)	32 μm (90%)

The theoretical volume of TMMC steered is based on the carrier cumulative size distribution.³⁹ In this simulation, several blood flow velocities are considered because it was not possible to measure the velocity prior to MRN without inducing damages to the hepatic artery.

TE (~4 ms) could be used during the initial embolization phase to detect TMMC in the targeted lobe. Sequences with higher TE (~10 ms) could be helpful to detect TMMC in the untargeted lobe and thus to prevent backflow at the end of embolization.

Future Design

The future challenge for MRN will be to control TMMC distribution through at least two bifurcations of the hepatic vascular network to reach HCC nodules. Furthermore, TMMC properties such as the diameter have to be adapted to the human scale. To introduce and illustrate the future constraints for TMMC design, the following case was used: MRN in the human PHA and then in the right hepatic artery (RHA) to target HCC nodules localized in the right liver lobe (Fig. 5a).

The following design study, based on theoretical V_{mag} value (Eq. (2)), took into consideration TMMC properties (nanoparticle nature and loading), MRN platform parameters (gradient amplitude and rise time (Fig. 5b) and human hepatic vascular network properties (Table 2).^{5,7,18,46} The catheter tip would be placed at the beginning of the first artery to cross, providing a longer distance for MRN. Hence, to determine t_{max} , the length of each hepatic artery was considered (Table 2).

The effect of these parameters on TMMC diameter was compared: the size of the carrier is a critical parameter for liver chemoembolization. Drug eluting beads ($\varnothing \approx 100\text{--}300 \mu\text{m}$) with sustained release of DOX induces a better liver tumor necrosis than larger DEB³² and a better tumor response was achieved with 100–300- μm embolic microparticles.^{2,22,44} Moreover, smaller microparticles should be used with caution; they could escape from the hepatic vascular network and reach the systemic circulation inducing serious secondary effects.²¹ Hence, for the MRN in the human liver, the diameter of the microcarriers should be around 300 μm to realize a distal chemoembolization of the tumor and to minimize systemic distribution.

Iron oxide (Fe₃O₄) and FeCo MNP were considered because of their high magnetic properties and their

biomedical applications, respectively (Table 2).³⁸ As shown in Table 3, the nature and the loading of nanoparticles will affect the diameter of the microcarrier. At human scale, the use of Fe₃O₄ nanoparticles seems not suitable, despite the increased volume of the particle. Even though the PHA may be crossed with a loading as low as 10% w/w, the crossing of the second artery will be extremely challenging, even with a loading higher than 40% w/w. The crossing of the RHA remains even more challenging, mainly due to shorter steering length and higher blood flow velocity (Fig. 5a; Table 2). However, with FeCo nanoparticles, MRN could be achieved with a loading slightly above 10% w/w. Therefore, to ensure the steering in both PHA and RHA, the loading of FeCo nanoparticles between 20 and 30% w/w should be considered to ensure efficient MRN. This loading value was used for the preclinical experiments and it has allowed compensating the various hepatic artery network configurations and the decrease of steering gradient amplitude due to animal size variation (Figs. 2 and 4).³⁹ Moreover, the encapsulation of highly magnetic nanoparticles into the carrier remains attractive to reduce the metal content in the carriers and it could lead to increase the drug loading.

The properties of the steering coils such as the gradient amplitude and the rise and fall time are critical parameters to consider. The rise time corresponds to the time to set the gradient from 0 mT m⁻¹ to the steering value. The fall time corresponds to the time to set back the gradient to 0 mT m⁻¹ (Fig. 5b). This time will depend on the properties of the steering coils and the safety limits for human interventions. In this design study, the same value of rise and fall time was considered (Table 2). The fall time was added to the steering time in the PHA to set the gradient at 0 mT m⁻¹ before TMMC reach the RHA. Then, the rise time was added to the steering time in the RHA to change the TMMC trajectory to HCC nodules (Fig. 5).

The gradient amplitude and the rise time will affect significantly the diameter of TMMC (Table 4). When the maximum gradient amplitude will decrease, the diameter should be increased to ensure efficient MRN.

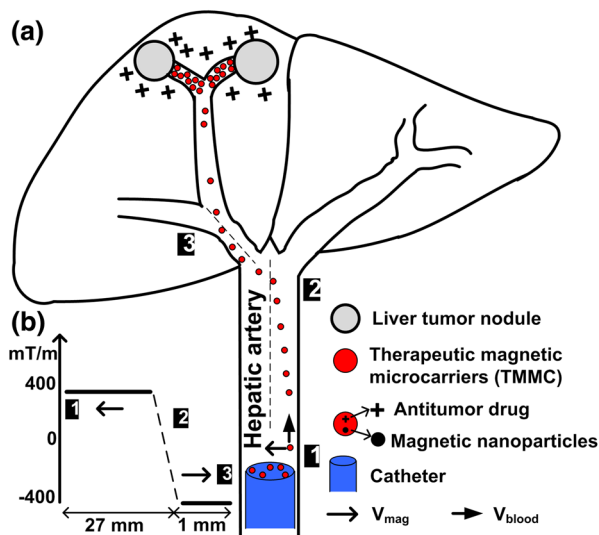


FIGURE 5. Schematic representation of the MRN of TMMC in the proper and right human hepatic artery to target HCC nodules (a) and theoretical variation of the steering gradient according to the pre-planned trajectory (b). The PHA and the RHA correspond to the section delimited by 1–2 and 2–3 on (a), respectively (NanoRobotics Laboratory, Ecole Polytechnique de Montréal).

TABLE 2. Parameters used to design TMMC for the theoretical MRN in the human proper and right hepatic arteries.

TMMC		
Nanoparticles (M_s , emu g^{-1})	FeCo (235) Fe ₃ O ₄ (90)	
Loading (% w/w)	10/20/30/40	
MRN platform		
Gradient (mT m^{-1})	200/300/400	
Rise time (ms)	0/10/30/50	
Hepatic artery parameters		
	PHA	RHA
Diameter (\varnothing , mm)	4.4	2.9
Length (L , mm)	27	7
V_{blood} (cm s^{-1})	28	31
t_{max} (ms)	95	22

t_{max} corresponds to the time required by TMMC dragged by the blood flow to reach the bifurcation.

Furthermore, in this case, if the rise time exceeds 15 ms to reach 400 $mT m^{-1}$, the TMMC diameter should be above 300 μm for MRN in the RHA. Hence, due to the high velocity of the blood flow and the short steering distance, the steering time will be more affected by the rise time in the RHA than in the PHA. As a reminder, if HCC nodules were supplied by the right bifurcation with the RHA, it would not have

TABLE 3. Theoretical TMMC diameter according to the nanoparticle nature and loading.

MNP and loading (% w/w)	TMMC M_s (emu g^{-1})	TMMC diameter (μm)	
		PHA	RHA
FeCo—10	23	174	317
FeCo—20	46	104	225
FeCo—30	69	85	183
FeCo—40	92	74	159
Fe ₃ O ₄ —10	9	299	645
Fe ₃ O ₄ —30	27	173	372
Fe ₃ O ₄ —40	36	150	323

A magnetic gradient of 400 $mT m^{-1}$ and a rise time of 10 ms were considered. The blood flow velocity was set at 28 $cm s^{-1}$ in PHA and at 31 $cm s^{-1}$ in RHA.

TABLE 4. Theoretical TMMC diameter according to the steering gradient and the rise time.

Gradient (mT m^{-1})	Rise time (ms)	TMMC diameter (μm)	
		PHA	RHA
200	5	117	218
200	10	120	259
300	7.5	97	193
300	10	88	212
400	0	81	136
400	10	85	183
400	15	88	240
400	20	91	449

A loading of 30%-FeCo nanoparticles into TMMC was considered. The blood flow velocity was set at 28 $cm s^{-1}$ in PHA and at 31 $cm s^{-1}$ in RHA.

been necessary to change the gradient amplitude and direction. Hence, the rise time will be set to zero. Thus, the TMMC diameter could be reduced by at least 25% (Table 4). These examples show that the future TMMC design should integrate the rise time value.

The effect of blood flow velocity on the carrier diameter was considered; the tumor can increase the blood flow velocity in the hepatic artery (Table 5).¹⁷ However, as for the MRN in the living rabbit, the blood flow velocity in the hepatic artery could be reduced by a balloon catheter.³⁹ According to Table 5, the diameter of the microcarriers will increase with the blood flow velocity in a linear way in PHA and in a logarithmical way in RHA. When the blood flow velocity will be decreased from 28 to 15 $cm s^{-1}$ by using a balloon catheter, TMMC diameter should decrease by 30%. By considering FeCo nanoparticles and 30%-loading, TMMC could be steered in the PHA and RHA with the different blood flow velocities considered.

TABLE 5. Theoretical TMMC diameter according to the blood flow velocity.

$V_{\text{blood PHA}}$ (cm s ⁻¹)	$V_{\text{blood RHA}}$ (cm s ⁻¹)	TMMC diameter (μm)	
		PHA	RHA
28	31	85	183
40	44	103	261
55	61	125	291
15	17	60	114

A loading of 30%-FeCo nanoparticles into TMMC, a steering gradient of 400 mT m⁻¹ and a rise time of 10 ms were taken into consideration.

This design study, based on the theoretical velocity of the TMMC acquired during MRN, shows the effects of different parameters on TMMC design for human-scale intervention. Future works will aim to improve this model by taking into considerations, among other, the spatial and temporal properties of the blood flow, the applied steering force during the rise and fall time and the particle concentration. Before conducting clinical applications, additional parameters have to be investigated. The potential magnetic aggregation during MRN should be evaluated; particle aggregates could be interesting for the steering,^{29,48} but they could also lead to healthy and tumor blood vessel embolization and thus limiting the therapeutic efficacy. An advanced model of the MRN should be developed to predict the steering efficiency.^{4,29,39} Real-time tracking and control of TMMC should be developed to adjust the gradient amplitude when required by the pre-planned trajectory. The safety of using a rise time of 10 ms and gradient amplitude of 400 mT m⁻¹ should be validated prior to develop human-scale steering gradient coils.²⁵ Furthermore, the biocompatibility of the carrier should be investigated *in vitro* and *in vivo*; magnetic materials without surface coating exhibit low corrosion parameters and metal ions could be released.^{40,42}

CONCLUSION

The design of carriers for endovascular MRN to target deep tissues was validated in animal models. The *in vivo* proof-of-concept confirmed the potential of MRN-compatible carriers to spare untargeted tissues from the therapeutic treatment. The steering in the vascular network worked because TMMC were designed by integrating several parameters. Based on the theoretical steering model, TMMC design for future MRN in human hepatic artery branches should integrate the following parameters: the properties of the targeted vascular network, the parameters of the

steering platform, the *in vivo* protocol and the nature and the loading of MNP. To optimize the targeting, the blood flow velocity should be reduced by a balloon catheter and the steering platform should possess high gradient amplitudes with a corresponding short rise and fall time. TMMC should be loaded with nanoparticles exhibiting M_s above 100 emu g⁻¹ to optimize the carrier diameter for efficient chemoembolization of HCC nodules.

ACKNOWLEDGMENTS

This work was supported by the Canadian Institutes for Health Research (CIHR), the Canada Research Chair program, the Canada Foundation for Innovation (CFI), the Natural Sciences and Engineering Research Council of Canada (NSERC), and Fonds Québécois de la Recherche sur la Nature et les Technologies (FQRNT).

REFERENCES

- Abbott, J. J., K. E. Peyer, M. C. Lagomarsino, Z. Li, D. Lixin, I. K. Kaliakatsos, and B. J. Nelson. How should microrobots swim? *Int. J. Robot. Res.* 28:1434–1447, 2009.
- Amesur, N. B., A. B. Zajko, and B. I. Carr. Chemoembolization for unresectable hepatocellular carcinoma with different sizes of embolization particles. *Dig. Dis. Sci.* 53:1400–1404, 2008.
- Amirfazli, A. Nanomedicine: magnetic nanoparticles hit the target. *Nat. Nanotechnol.* 2:467–468, 2007.
- Arcese, L., M. Fruchard, and A. Ferreira. Endovascular magnetically guided robots: navigation modeling and optimization. *IEEE Trans. Biomed. Eng.* 59:977–987, 2012.
- Basciano, C. A., C. Kleinstreuer, A. S. Kennedy, W. A. Dezarn, and E. Childress. Computer modeling of controlled microsphere release and targeting in a representative hepatic artery system. *Ann. Biomed. Eng.* 38:1862–1879, 2010.
- Bruix, J., and J. M. Llovet. Major achievements in hepatocellular carcinoma. *Lancet* 373:614–616, 2009.
- Carlisle, K. M., M. Halliwell, A. E. Read, and P. N. Wells. Estimation of total hepatic blood flow by duplex ultrasound. *Gut* 33:92–97, 1992.
- Chanu, A., O. Felfoul, G. Beaudoin, and S. Martel. Adapting the clinical MRI software environment for real-time navigation of an endovascular untethered ferromagnetic bead for future endovascular interventions. *Magn. Reson. Med.* 59:1287–1297, 2008.
- Chorny, M., I. Fishbein, B. B. Yellen, I. S. Alferiev, M. Bakay, S. Ganta, R. Adamo, M. Amiji, G. Friedman, and R. J. Levy. Targeting stents with local delivery of paclitaxel-loaded magnetic nanoparticles using uniform fields. *Proc. Natl Acad. Sci. U.S.A.* 107:8346–8351, 2010.
- Dames, P., B. Gleich, A. Flemmer, K. Hajek, N. Seidl, F. Wiekhorst, D. Eberbeck, I. Bittmann, C. Bergemann, T. Weyh, L. Trahms, J. Rosenecker, and C. Rudolph. Tar-

- geted delivery of magnetic aerosol droplets to the lung. *Nat. Nanotechnol.* 2:495–499, 2007.
- ¹¹Darton, N. J., A. J. Sederman, A. Ionescu, C. Ducati, R. C. Darton, L. F. Gladden, and N. K. H. Slater. Manipulation and tracking of superparamagnetic nanoparticles using MRI. *Nanotechnology* 19:395102, 2008.
 - ¹²Di Bisceglie, A. M. Epidemiology and clinical presentation of hepatocellular carcinoma. *J. Vasc. Interv. Radiol.* 13:S169–S171, 2002.
 - ¹³Dobson, J. Cancer therapy: a twist on tumour targeting. *Nat. Mater.* 9:95–96, 2010.
 - ¹⁴Felfoul, O., J. B. Mathieu, G. Beaudoin, and S. Martel. In vivo MR-tracking based on magnetic signature selective excitation. *IEEE Trans. Med. Imaging* 27:28–35, 2008.
 - ¹⁵Frutiger, D. R., K. Vollmers, B. E. Kratochvil, and B. J. Nelson. Small, fast, and under control: wireless resonant magnetic micro-agents. *Int. J. Robot. Res.* 29:613–636, 2010.
 - ¹⁶Gosselin, F. P., V. Lalande, and S. Martel. Characterization of the deflections of a catheter steered using a magnetic resonance imaging system. *Med. Phys.* 38:4994–5002, 2011.
 - ¹⁷Jakab, F., Z. Rath, F. Schmal, P. Nagy, and J. Faller. Changes in hepatic hemodynamics due to primary liver tumours. *HPB Surg.* 9:245–248, 1996.
 - ¹⁸Jakab, F., Z. Rath, F. Schmal, P. Nagy, and J. Faller. A new method to measure portal venous and hepatic arterial blood flow in patients intraoperatively. *HPB Surg.* 9:239–243, 1996.
 - ¹⁹Konya, A., K. C. Wright, I. A. Szwarc, and R. D. Collins. Technical aspects of catheter-related interventions in the liver of the rabbit. *Acta Radiol.* 38:332–334, 1997.
 - ²⁰Kósa, G., P. Jakab, G. Székely, and N. Hata. MRI driven magnetic microswimmers. *Biomed. Microdevices* 14:165–178, 2012.
 - ²¹Lencioni, R., T. de Baere, M. Burrell, J. G. Caridi, J. Lammer, K. Malagari, R. C. Martin, E. O'Grady, M. I. Real, T. J. Vogl, A. Watkinson, and J. F. Geschwind. Transcatheter treatment of hepatocellular carcinoma with doxorubicin-loaded DC bead (DEBDOX): technical recommendations. *Cardiovasc. Interv. Radiol.* 35:980–985, 2011.
 - ²²Liapi, E., and J. F. Geschwind. Transcatheter and ablative therapeutic approaches for solid malignancies. *J. Clin. Oncol.* 25:978–986, 2007.
 - ²³Lin, R., L. Shi Ng, and C. H. Wang. In vitro study of anticancer drug doxorubicin in PLGA-based microparticles. *Biomaterials* 26:4476–4485, 2005.
 - ²⁴Lubbe, A. S., C. Bergemann, H. Riess, F. Schriever, P. Reichardt, K. Possinger, M. Matthias, B. Dorken, F. Herrmann, R. Gurtler, P. Hohenberger, N. Haas, R. Sohr, B. Sander, A. J. Lemke, D. Ohlendorf, W. Huhnt, and D. Huhn. Clinical experiences with magnetic drug targeting: a phase I study with 4'-epidoxorubicin in 14 patients with advanced solid tumors. *Cancer Res.* 56:4686–4693, 1996.
 - ²⁵Martel, S. Combining pulsed and DC gradients in a clinical MRI-based microrobotic platform to guide therapeutic magnetic agents in the vascular network. *Int. J. Robot. Res.* 10:7, 2012.
 - ²⁶Martel, S., O. Felfoul, J. B. Mathieu, A. Chanu, S. Tamaz, M. Mohammadi, M. Mankiewicz, and N. Tabatabaei. MRI-based medical nanorobotic platform for the control of magnetic nanoparticles and flagellated bacteria for target interventions in human capillaries. *Int. J. Robot. Res.* 28:1169–1182, 2009.
 - ²⁷Martel, S., J. B. Mathieu, O. Felfoul, A. Chanu, E. Aboussouan, S. Tamaz, P. Pouponneau, L. Yahia, G. Beaudoin, G. Soulez, and M. Mankiewicz. Automatic navigation of an untethered device in the artery of a living animal using a conventional clinical magnetic resonance imaging system. *Appl. Phys. Lett.* 90:114105, 2007.
 - ²⁸Martel, S., J. B. Mathieu, O. Felfoul, A. Chanu, E. Aboussouan, S. Tamaz, P. Pouponneau, L. Yahia, G. Beaudoin, G. Soulez, and M. Mankiewicz. A computer-assisted protocol for endovascular target interventions using a clinical MRI system for controlling untethered microdevices and future nanorobots. *Comput. Aided Surg.* 13:340–352, 2008.
 - ²⁹Mathieu, J. B., and S. Martel. Steering of aggregating magnetic microparticles using propulsion gradients coils in an MRI Scanner. *Magn. Reson. Med.* 63:1336–1345, 2010.
 - ³⁰Nacev, A., A. Komae, A. Sarwar, R. Probst, S. H. Kim, M. Emmert-Buck, and B. Shapiro. Towards control of magnetic fluids in patients: directing therapeutic nanoparticles to disease locations. *IEEE Contr. Syst. Mag.* 32:43, 2012.
 - ³¹Namiki, Y., T. Namiki, H. Yoshida, Y. Ishii, A. Tsubota, S. Koido, K. Nariai, M. Mitsunaga, S. Yanagisawa, H. Kashiwagi, Y. Mabashi, Y. Yumoto, S. Hoshina, K. Fujise, and N. Tada. A novel magnetic crystal-lipid nanostructure for magnetically guided in vivo gene delivery. *Nat. Nanotechnol.* 4:598–606, 2009.
 - ³²Namur, J., M. Wassef, J. M. Millot, A. L. Lewis, M. Manfait, and A. Laurent. Drug-eluting beads for liver embolization: concentration of doxorubicin in tissue and in beads in a pig model. *J. Vasc. Interv. Radiol.* 21:259–267, 2010.
 - ³³Nelson, B. J., I. K. Kaliakatsos, and J. J. Abbott. Microrobots for minimally invasive medicine. *Annu. Rev. Biomed. Eng.* 12:55–85, 2010.
 - ³⁴Noar, J. H., R. D. Evans, D. Wilson, J. Costello, E. Ioannou, A. Ayeni, N. J. Mordan, M. Wilson, and J. Pratten. An in vitro study into the corrosion of intra-oral magnets in the presence of dental amalgam. *Eur. J. Orthod.* 25:615–619, 2003.
 - ³⁵Park, S., K. Cha, and J. Park. Development of biomedical microrobot for intravascular therapy. *Int. J. Robot. Res.* 7:97–98, 2010.
 - ³⁶Plank, C. Nanomedicine: silence the target. *Nat. Nanotechnol.* 4:544–545, 2009.
 - ³⁷Polyak, B., I. Fishbein, M. Chorny, I. Alferiev, D. Williams, B. Yellen, G. Friedman, and R. J. Levy. High field gradient targeting of magnetic nanoparticle-loaded endothelial cells to the surfaces of steel stents. *Proc. Natl Acad. Sci. U.S.A.* 105:698–703, 2008.
 - ³⁸Pouponneau, P., J. C. Leroux, and S. Martel. Magnetic nanoparticles encapsulated into biodegradable microparticles steered with an upgraded magnetic resonance imaging system for tumor chemoembolization. *Biomaterials* 30:6327–6332, 2009.
 - ³⁹Pouponneau, P., J. C. Leroux, G. Soulez, L. Gaboury, and S. Martel. Co-encapsulation of magnetic nanoparticles and doxorubicin into biodegradable microcarriers for deep tissue targeting by vascular MRI navigation. *Biomaterials* 32:3481–3486, 2011.
 - ⁴⁰Pouponneau, P., O. Savadogo, T. Napporn, L. Yahia, and S. Martel. Corrosion study of iron-cobalt alloys for MRI-based propulsion embedded in untethered microdevices operating in the vascular network. *J. Biomed. Mater. Res. B* 93:203–211, 2010.
 - ⁴¹Pouponneau, P., O. Savadogo, T. Napporn, L. Yahia, and S. Martel. Corrosion study of single crystal Ni-Mn-Ga al-

- loy and Tb_{0.27}Dy_{0.73}Fe_{1.95} alloy for the design of new medical microdevices. *J. Mater. Sci. Mater. Med.* 22:237–245, 2011.
- ⁴²Pouponneau, P., V. Segura, O. Savadogo, J.-C. Leroux, and S. Martel. Annealing of magnetic nanoparticles for their encapsulation into microcarriers guided by vascular magnetic resonance navigation. *J. Nanopart. Res.* 14:1–13, 2012.
- ⁴³Pouponneau, P., G. Soulez, G. Beaudoin, J. C. Leroux, and S. Martel. MR imaging of therapeutic magnetic microcarriers guided by magnetic resonance navigation for targeted liver chemoembolization. *Cardiovasc. Interv. Radiol.* DOI: [10.1007/s00270-013-0770-4](https://doi.org/10.1007/s00270-013-0770-4), 2013.
- ⁴⁴Reyes, D. K., J. A. Vossen, I. R. Kamel, N. S. Azad, T. A. Wahlin, Torbenson, MS, M. A. Choti, and J. F. Geschwind. Single-center phase II trial of transarterial chemoembolization with drug-eluting beads for patients with unresectable hepatocellular carcinoma: initial experience in the United States. *Cancer J.* 15:526–532, 2009.
- ⁴⁵Riegler, J., J. A. Wells, P. G. Kyrtatos, A. N. Price, Q. A. Pankhurst, and M. F. Lythgoe. Targeted magnetic delivery and tracking of cells using a magnetic resonance imaging system. *Biomaterials* 31:5366–5371, 2010.
- ⁴⁶Silveira, L. A., F. B. Silveira, and V. P. Fazan. Arterial diameter of the celiac trunk and its branches. Anatomical study. *Acta Cir. Bras.* 24:43–47, 2009.
- ⁴⁷Tamaz, S., R. Gourdeau, A. Chanu, J. B. Mathieu, and S. Martel. Real-time MRI-based control of a ferromagnetic core for endovascular navigation. *IEEE Trans. Biomed. Eng.* 55:1854–1863, 2008.
- ⁴⁸Vartholomeos, P., and C. Mavroidis. In silico studies of magnetic microparticle aggregations in fluid environments for MRI-guided drug delivery. *IEEE Trans. Biomed. Eng.* 59:3028–3038, 2012.
- ⁴⁹Yesin, K. B., K. Vollmers, and B. J. Nelson. Modeling and control of untethered biomicrobots in a fluidic environment using electromagnetic fields. *Int. J. Robot. Res.* 25:527–536, 2006.